Influence of Alloyed Sn on Adsorption and Reaction of NO on Pt(100) Surfaces

Chameli Panja and Bruce E. Koel*

Department of Chemistry, University of Southern California, Los Angeles, California 90089-0482

Received: September 29, 1999; In Final Form: December 1, 1999

Adsorption and reaction of NO on the (5 × 20)-Pt(100) surface and two Sn/Pt(100) surface alloys have been studied using temperature programmed desorption (TPD) and high-resolution electron energy loss spectroscopy (HREELS). On the (5 × 20)-Pt(100) surface, in the absence of Sn, NO is primarily reversibly adsorbed, and most of the chemisorbed NO desorbs molecularly from the surface during TPD. Approximately 25% of the adsorbed NO monolayer decomposes at temperatures higher than 400 K, and this leads to N_2 and O_2 desorption from the surface. Alloying Sn into the surface layer of Pt(100) forms two ordered surface alloys having c(2 × 2) and (3$\sqrt{2}$ × $\sqrt{2}$)R45°Sn/Pt(100) surface structures with $\theta_{Sn} = 0.5$ and 0.67 ML, respectively. Alloying reduced the saturation coverage of NO in the chemisorbed monolayer from that on Pt(100) at 100 K, and it also reduced the adsorption energy of molecularly bound NO by more than a factor of 2. Alloyed Sn, which removes all pure-Pt 2-fold bridge and 4-fold hollow sites, completely changed the NO reaction pathway: nitrogen in NO was partially reduced to form N_2O on these alloys so that N_2O, along with NO and O_2, desorption was observed in TPD. NO is bonded at the same site with a similar geometry on both Pt(100) and the Sn/Pt(100) alloyed surfaces at low NO coverages, based on the HREELS spectra. At saturation (monolayer) coverages, however, quite different HREELS spectra were observed on both of the Sn/Pt(100) alloyed surfaces compared to that on Pt(100). Vibrations were observed from adsorbed N_2O, along with a shift of more than 60 cm^{-1} for two ν_{NO} peaks on both of the Sn/Pt(100) alloys compared to Pt(100). The two ν_{NO} peaks can be assigned either as (i) two ν_s modes of bent (tilted) and linearly bonded atop NO or as (ii) ν_s and ν_{as} stretching modes of a surface dinitrosyl species, that is, two NO molecules bound to one Pt atom. Dinitrosyl species have been proposed as intermediates for N_2O formation in reactions of NO on Mo(110) (Queeney and Friend, *J. Chem. Phys.* **1997**, *107*, 6432), and we suggest that a similar reaction mechanism occurs on Sn/Pt(100) alloys.

1. Introduction

Nitric oxide (NO) adsorption and reaction on transition-metal surfaces is of fundamental and technological interest.[1−4] As one example, catalytic removal of NO_x from combustion emissions is a crucial air pollution control problem because NO favors the photochemical formation of ozone in the lower atmosphere and is also a "green house" gas.[5] Catalysts for NO reduction are typically supported transition metals, and so, NO adsorption and chemistry on transition metal surfaces is at the heart of this catalysis.

Pt and Rh are good metals for NO reduction,[6,7] but Pt−Rh bimetallic catalysts outperform both Pt and Rh catalysts to simultaneously remove NO_x, CO, and hydrocarbons from automotive exhaust gases in catalytic converters.[8,9] This is not surprising because bimetallic catalysts often have strikingly different performances in catalytic processes compared to their single metal component systems.[10,11] The activity for NO + CO reactions is enhanced on Pd−Cu[12] and Pd−Cr[13] bimetallic surfaces, compared to Pd alone, and it has been suggested that the main reason is because of the more facile NO dissociation on the bimetallic Pd surfaces, compared to pure Pd surfaces.[12,13]

Surface science studies have shown that the catalytic activity of Pt surfaces in the CO + NO reaction is related to the efficiency of dissociation of NO, which varies for different crystal planes.[14] For example, NO partially decomposes to yield N_2 and O_2 on the Pt(100) surface,[15−18] whereas no dissociation occurs on Pt(111).[16,19,20] HREELS and infrared reflection absorption spectroscopy (IRAS) studies show that NO adsorbs molecularly on the reconstructed hex-Pt(100) surface at room temperature, but it initially adsorbs dissociatively on the (1 × 1)-Pt(100) surface prior to molecular adsorption at higher NO coverages.[15,17,18]

The clean Pt(100) surface reconstructs to expose a "quasi-hexagonal", close-packed outermost layer with a (5 × 20) unit cell and a stable Pt(100)-hex-R0.7° layer when the first phase is annealed above 1100 K.[21] This is generally known as the "hex" phase and has been characterized by many techniques.[21−23] Adsorption of small molecules, such as H_2,[24] CO,[25−27] or NO,[27−30] induce a phase transition from the hex structure to a "square" (1 × 1)-Pt(100) structure with a unit cell, as expected, from the ideal termination of the bulk lattice. Such adsorbate-induced phase transitions play a role in the mechanism of several oscillatory reactions on Pt(100).[25−30]

On the hex-Pt(100) surface, at temperatures between 200 and 300 K, NO adsorption immediately lifts the reconstruction to form NO-covered (1 × 1)-islands.[27−30] At temperatures below 200 K, adsorption does not immediately lift the reconstruction, and this results in significant NO accumulation directly on the hex phase. A temperature-dependent critical coverage of NO is required for the structural phase transition to occur.[29]

To probe the adsorption and reaction site requirements on bimetallic Pt surfaces, we have been exploring the influence of Sn on Pt surface chemistry. We have previously studied NO

* To whom correspondence should be addressed.

10.1021/jp993495r CCC: $19.00
Published on Web 02/25/2000

adsorption on two ordered Sn/Pt(111) surface alloys.[20] Alloying the Pt(111) surface layer with Sn reduced the binding energy of the most strongly bound NO chemisorbed on Pt(111) from 92 kJ/mol to 58 and 50 kJ/mol on the (2 × 2)Sn/Pt(111) and the ($\sqrt{3}$ × $\sqrt{3}$)R30° Sn/Pt(111) alloys, respectively. No dissociation of NO occurred on Pt(111) or either of these alloyed surfaces during TPD. Alloying with Sn reduced the saturation monolayer coverage of NO from 0.5 ML on Pt(111) to 0.4 ML on the (2 × 2) alloy and to 0.3 ML on the ($\sqrt{3}$ × $\sqrt{3}$)R30° Sn/Pt(111) alloy, at 100 K.[20]

Two additional, ordered Sn/Pt(100) alloys can be prepared by deposition and annealing of thin Sn films on Pt(100) single-crystal substrates in ultrahigh vacuum (UHV).[31,32] These alloys have surface nets giving c(2 × 2) and p(3$\sqrt{2}$ × $\sqrt{2}$)R45° low energy electron diffraction (LEED) patterns and have θ_{Sn} = 0.5 and ~0.67 ML, respectively. The structure and composition of the Sn/Pt(100) alloys formed on Pt(100) are quite different than the two Sn/Pt(111) alloys that were previously investigated.[20] The c(2 × 2) alloy removes all pure-Pt 2-fold bridge and 4-fold hollow sites. Hence, chemisorption studies of NO on these two Sn/Pt(100) alloy surfaces provide essential information on the roles that surface structure and composition play in tailoring the surface chemistry of Pt−Sn and other bimetallic Pt alloys.

2. Experimental Methods

These experiments were performed in a stainless steel UHV chamber that has been described previously[33] with an operating base pressure of 2 × 10^{-10} Torr. Briefly, it was equipped with LEED optics, a cylindrical mirror analyzer (CMA), for Auger electron spectroscopy (AES), an ion sputtering gun, a UTI 100C quadrupole mass spectrometer (QMS) for TPD, a HREELS spectrometer containing single-127° cylindrical sectors in the monochromator and analyzer, and facilities for gas dosing and metal evaporation.

The Pt(100) crystal was cleaned by repeated cycles of Ar^+ ion-sputtering and oxygen treatments (P_{O_2} = 5 × 10^{-7} Torr at 1200 K for 2 min), and then it was heated in a vacuum to 1240 K for 30 s. The cleanliness of the crystal was checked by AES and LEED. The clean surface showed a reconstructed (5 × 20)-Pt(100) pattern.[21−23] The crystal was resistively heated to 1250 K and cooled to 95 K by liquid nitrogen, with the temperature measured by a chromel−alumel thermocouple spot-welded to the side of the crystal.

NO exposures were carried out by using a leak valve connected to a multichannnel-array gas doser. NO (Matheson, 99.5% purity) was used without further purification. The exposures of NO are given herein in units of langmuirs, corrected for ionization gauge sensitivity (S_{NO}/S_{N_2} = 1.3) and a gas-doser flux enhancement factor (45 over that for the background gas flux).

All of the TPD experiments were done with a heating rate of 4 K/s. HREELS spectra were taken in specular reflection with $\theta_{in} = \theta_{out} = 65°$ from the surface normal. The electron-incident energy in HREELS was 4.5 eV, with a typical resolution of 70−80 cm^{-1} from clean Pt(100).

The c(2 × 2) and (3$\sqrt{2}$ × $\sqrt{2}$)R45° Sn/Pt(100) surface alloys were prepared by evaporating Sn on the clean, reconstructed (5 × 20)-Pt(100) surface at 300 K and then annealing to 750 and 900 K, respectively.[31,32] The c(2 × 2) LEED pattern observed following Sn deposition on Pt(100) can be due to two different surface structures.[31,32] A c(2 × 2)-Sn overlayer (comprising Sn adatoms) is formed over the temperature range of 500−750 K.[31] A c(2 × 2) alloy is formed by the substitutional incorporation of Sn into Pt sites in the outermost layer over a narrow range between 750 and 800 K, depending on the initial Sn concentration. A more thermally stable alloy with a (3$\sqrt{2}$ × $\sqrt{2}$)R45° LEED pattern is formed at higher annealing temperatures of over 800 K, and this structure is stable up to 1050 K. The structure and composition of the c(2 × 2) alloy has been determined by low energy alkali ion scattering spectroscopy (ALISS).[32] This surface has θ_{Sn} = 0.5 ML and is quite "flat", with an outward buckling distance of 0.19 ± 0.02 Å for Sn atoms above the surface Pt plane.[32] ALISS revealed that an alloy, with a similar local geometric structure to the c(2 × 2) alloy and composed of small c(2 × 2) alloy domains with the same Sn-buckling distance within the domains, was also formed for the (3$\sqrt{2}$ × $\sqrt{2}$)R45° LEED pattern.[32] The surface Sn coverage in the (3$\sqrt{2}$ × $\sqrt{2}$)R45° Sn/Pt(100) alloy was estimated to be 0.67 ML. Paffett et al.[31] suggested that this surface was faceted with Sn-rich domain boundaries. Recently, in what may be a closely related structure, STM images of the (100) surface of a bulk Pt_3Sn alloy crystal show pyramidal features consisting of (102) facets and terraces between and on top of the pyramidal facets after sputtering and annealing the surface to 600 K.[34] For brevity, the c(2 × 2)Sn/Pt(100) and (3$\sqrt{2}$ × $\sqrt{2}$)R45°Sn/Pt(100) surface alloys will be referred to simply as the c(2 × 2) and 3$\sqrt{2}$ alloys, respectively, throughout this paper.

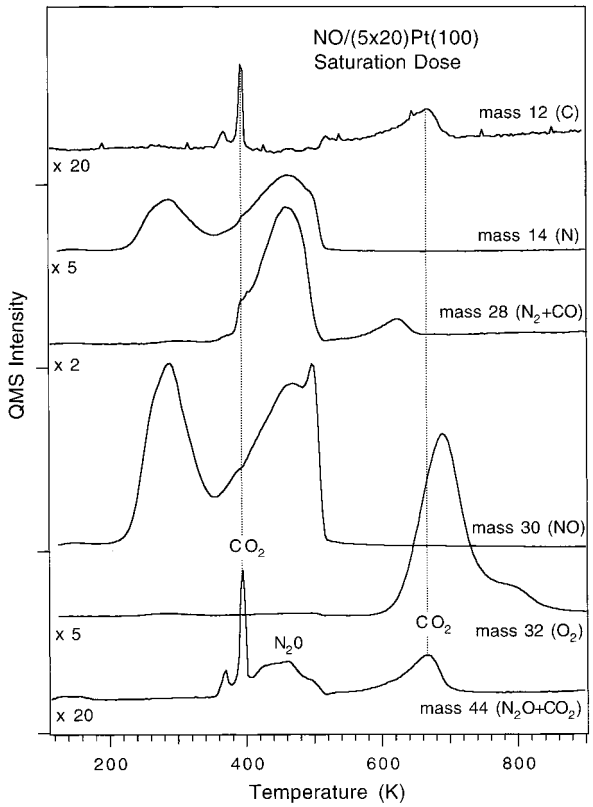

Figure 1. TPD curves used to identify products from the reaction of an NO monolayer on the hex-Pt(100) surface at 100 K.

3. Results

3.1. TPD. The principle desorption signals from the reaction of a NO monolayer during TPD on the hex-Pt(100) surface are shown in Figure 1. These curves were obtained simultaneously following adsorption of a saturation dose of NO on a clean, hex-Pt(100) surface at 100 K. Signals for C (12 amu) and N (14 amu) spectra can be used to distinguish the N_2 (28 amu) and N_2O (44 amu) desorption products of NO dissociation from

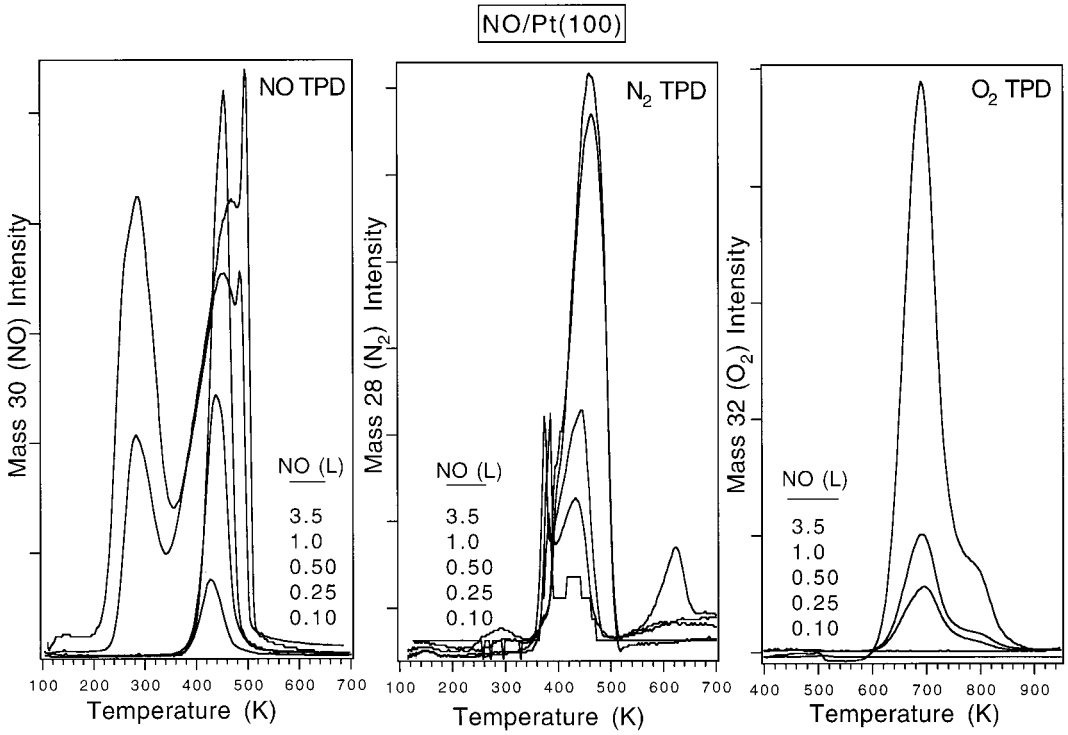

Figure 2. NO, N_2, and O_2 TPD traces following NO exposures on the hex-Pt(100) surface.

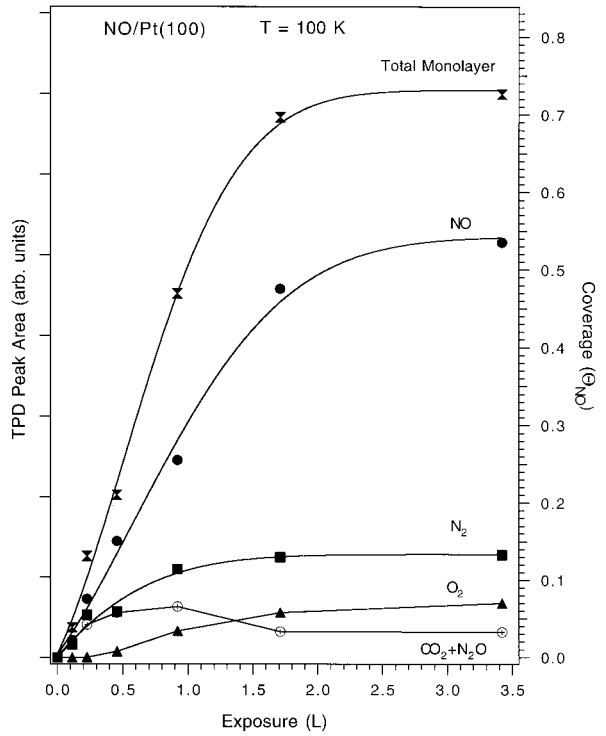

Figure 3. Uptake curves constructed from TPD results detailing NO adsorption kinetics on hex-Pt(100) at 100 K. The value for θ_{NO}^{sat} on Pt(100) was set to 0.73 ML.[29]

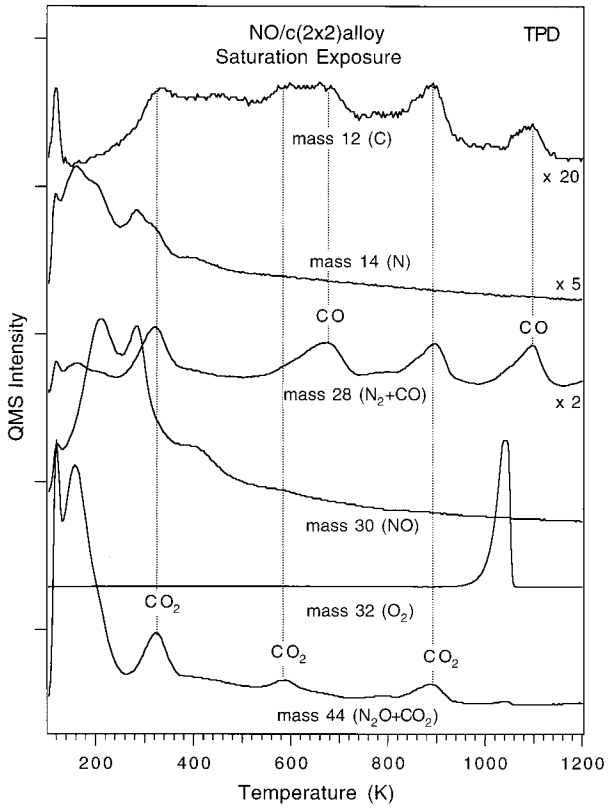

Figure 4. TPD traces from an NO monolayer on the c(2 × 2)Sn/Pt-(100) alloy at 100 K.

CO (28 amu) and CO_2 (44 amu) contamination. Most of the adsorbed NO desorbed molecularly from the surface, but ~25% (as determined below) of the NO at monolayer coverage decomposes during TPD to give mainly N_2 and O_2 desorption products, with a small amount of N_2O desorption also detected.

NO, N_2, and O_2 TPD curves following increasing NO exposures on the hex-Pt(100) surface at 100 K are shown in Figure 2. Overall, these data are consistent with that reported previously.[15−17] At low coverages, NO desorbs in a single peak at 430 K. This shifts to higher temperature with increasing initial NO coverage, and a high-temperature shoulder occurs at 500 K. The peak at 500 K does not grow until the main peak at 470 K saturates. The same phenomena, that is, the shifting of the desorption peak to a higher temperature and nonsequential filling of desorption states with increasing coverage, also occurred for adsorbed CO on hex-Pt(100). This behavior was

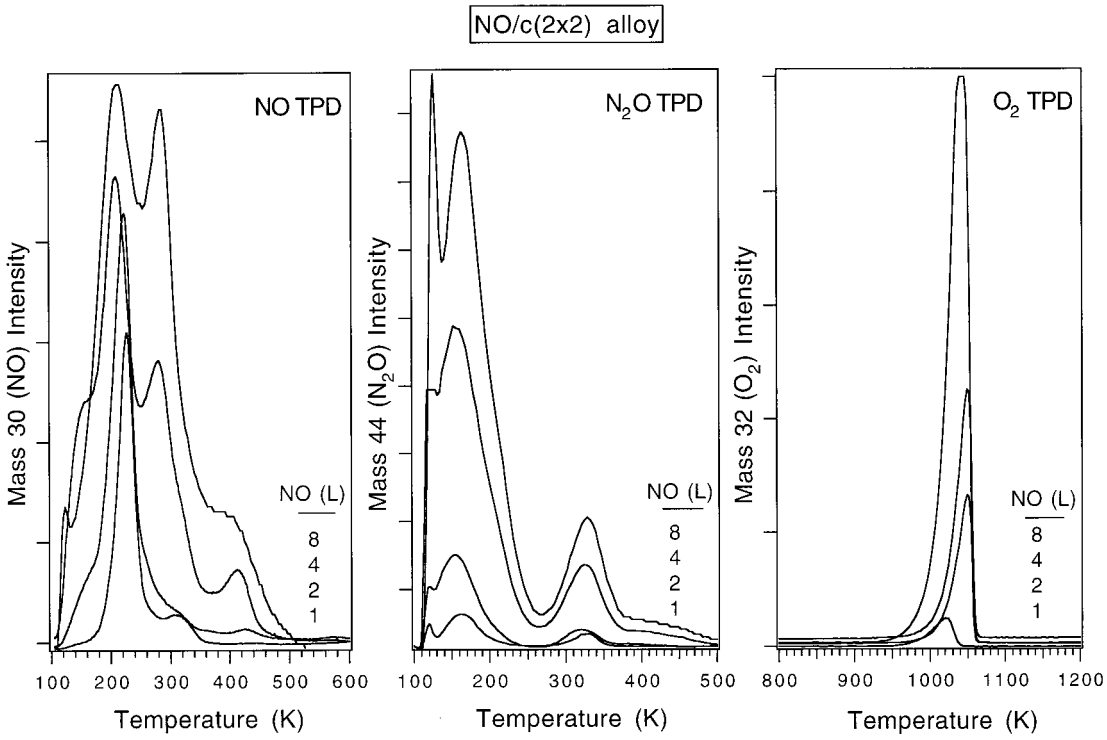

Figure 5. NO, N_2O, and O_2 TPD traces obtained after NO exposures on the c(2 × 2) Sn/Pt(100) alloy at 100 K.

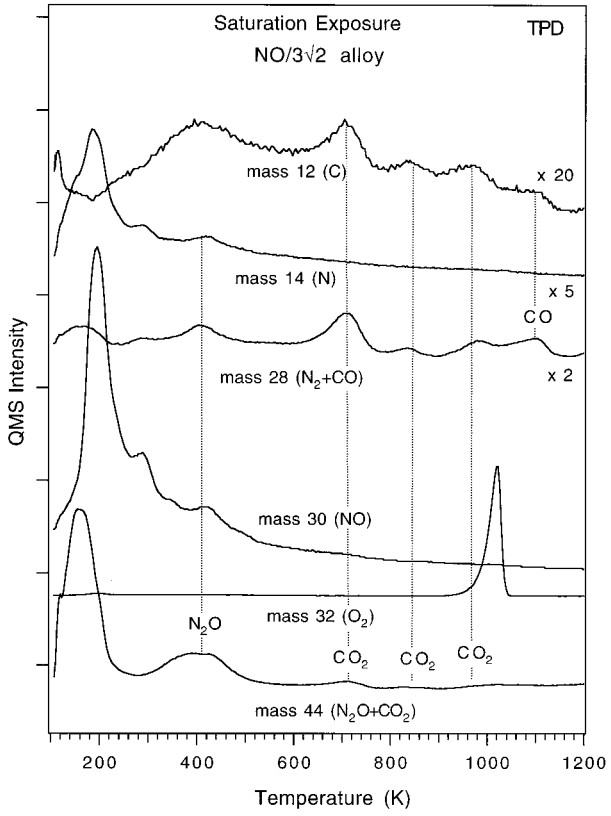

Figure 6. TPD curves from an NO monolayer on the (3√2 × √2)-R45°Sn/Pt(100) alloy at 100 K.

attributed to reconstruction of the hex phase to the (1 × 1)-Pt-(100) surface.[25,26] At higher initial NO coverages, a low-temperature NO desorption peak appeared at 288 K, which shifted to a lower temperature with increasing NO exposure. N_2 desorbed in a single peak at 465 K, with a low-temperature shoulder around 390 K. The peak at 465 K also shifted to higher temperature with increasing NO exposures. Molecular oxygen did not initially desorb from the surface, but eventually a peak was observed at 650 K along with a shoulder at 800 K.

Figure 3 provides the NO adsorption kinetics and shows the changes in the nature of reversible adsorption and reaction that occur with increasing NO coverage. The amounts of NO that desorbed or decomposed into other products were constructed from TPD peak areas after NO exposures on the hex-Pt(100) surface at 100 K. Following small NO exposures, most of the oxygen formed by NO dissociation reacted with small amounts of coadsorbed CO to form CO_2, and little oxygen desorbed from the surface. Some reversible adsorption and, thus, desorption of NO, occurred even at low coverages. At monolayer coverage of NO, about 75% of the adsorbed NO desorbed from the surface without dissociation. The NO coverage scale was referenced to the saturation coverage of NO, reported to be $\theta_{NO}^{sat} = 0.73$ ML on hex-Pt(100) at 100 K. This assumes 50% reversible adsorption for $\theta_{NO} = 0.5$ ML, which is associated with the saturation of the NO desorption peak at 470 K.[16,29] This calibration can be checked independently by referencing the O_2 TPD peak area from NO dissociation to that for an oxygen coverage, of $\theta_O = 2.2$ ML,[35] that was created by a saturation exposure of ozone (O_3) on the Pt(100) surface at 300 K. The results of this comparison were consistent.

TPD curves, after a saturation exposure of NO on the c(2 × 2) alloy at 100 K, are shown in Figure 4. The main desorbed products were N_2O (44 amu), NO (30 amu), and O_2 (32 amu) in contrast to that on Pt(100). Small, contaminant CO and CO_2 desorption peaks were identified by comparing all of the other TPD signals. Coadsorbed CO and carbon, which were present on the surface, reacted with oxygen to produce reaction-rate limited CO and CO_2 desorption. Almost no N_2 production from the reaction of NO on the alloyed surface was found.

Figure 5 shows TPD curves for NO, N_2O, and O_2 desorption products for increasing exposures of NO on the c(2 × 2) alloy at 100 K. At low coverages, NO desorbed in a large peak at 210 K and a smaller peak at 320 K. With increasing coverage,

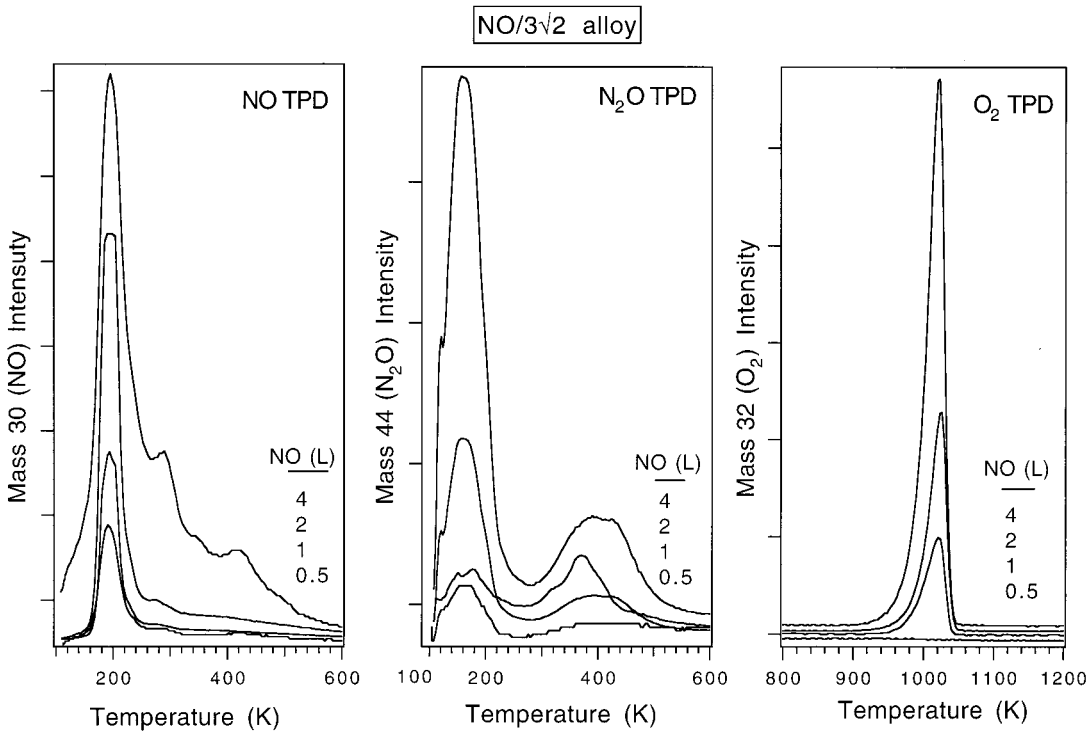

Figure 7. NO, N_2O, and O_2 TPD traces obtained following NO exposures on the $(3\sqrt{2} \times \sqrt{2})$R45°Sn/Pt(100) alloy at 100 K.

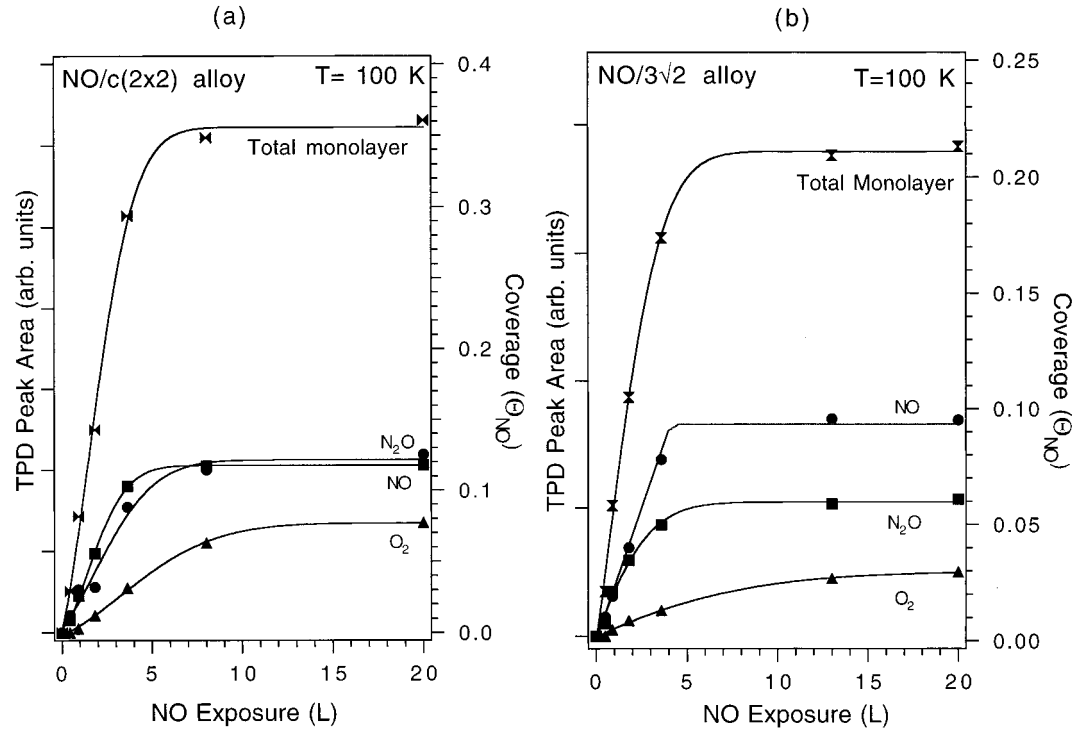

Figure 8. Uptake curves obtained from TPD results for NO adsorption kinetics at 100 K on (a) the c(2 × 2) Sn/Pt(100) alloy and (b) the $(3\sqrt{2} \times \sqrt{2})$R45°Sn/Pt(100) alloy.

NO desorption shifted to a lower temperature, probably because of NO−NO repulsive interactions. At high coverages, the peak at 320 K became relatively large and a new peak appeared at 420 K. N_2O desorbed in a single peak at 150 K (all other, higher temperature peaks were from CO_2 desorption). O_2 desorbed in a peak at 1030−1045 K. This high-temperature state has been assigned to the reduction of oxidized Sn in previous studies of the oxidation of these Pt−Sn alloys.[35]

TPD, as shown in Figure 6, was used after a saturation exposure of NO on the $3\sqrt{2}$ alloy at 100 K, to identify all desorbed products. As on the c(2 × 2) alloy, NO, N_2O, and O_2 were the main desorbed species. Although the amount of molecular NO adsorption was lower on the $3\sqrt{2}$ alloy than on the c(2 × 2) alloy, the fraction of adsorbed NO that desorbed as NO was higher on the $3\sqrt{2}$ alloy (vide infra).

Figure 7 shows a series of NO, N_2O, and O_2 TPD traces for increasing NO exposures on the $3\sqrt{2}$ alloy at 100 K. For all of the products, the peak shapes were very similar to those on the c(2 × 2) alloy, but the peak temperatures were slightly lower. This indicates a weaker interaction with the surface due to the

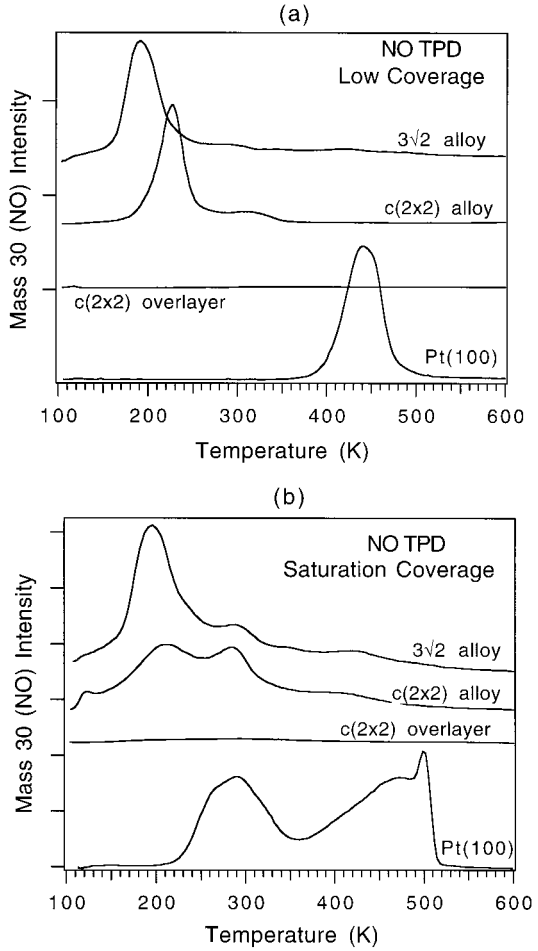

Figure 9. Comparison of NO TPD results from hex-Pt(100), the two alloys, and a c(2 × 2) overlayer at two coverages of NO (a) $\theta_{NO} = 0.1\ \theta_{NO}^{sat}$ and (b) $\theta_{NO} = \theta_{NO}^{sat}$ at 100 K on each surface.

larger amount of surface Sn on the $3\sqrt{2}$ alloy. This suggests a similar NO chemistry on these two alloys.

Uptake curves characterizing NO adsorption kinetics and the extent of reversible adsorption are shown in Figure 8 , parts a and b. NO TPD peak areas provide the amount of reversible NO adsorption, and this was found to be 0.12 and 0.09 ML on the c(2 × 2) and the $3\sqrt{2}$ alloys, respectively. O_2 TPD peak areas indicate that $\theta_O = 0.06$ and 0.03 ML on the c(2 × 2) and $3\sqrt{2}$ alloys, respectively, and desorb as O_2 at saturation NO coverage. On the c(2 × 2) alloy, about 70% of the adsorbed NO at saturation coverage reacted to eventually desorb N_2O and O_2 and 30% desorbed molecularly. For the $3\sqrt{2}$ alloy, about 40% of the adsorbed NO desorbed molecularly and 60% reacted to desorb N_2O and O_2. Alloyed Sn reduced the monolayer saturation coverage for NO from $\theta_{NO}^{sat} = 0.73$ ML on Pt(100) to $\theta_{NO}^{sat} = 0.35$ and 0.22 ML on the c(2 × 2) and $3\sqrt{2}$ alloys, respectively.

The initial slopes of the uptake curves are proportional to the initial sticking coefficient (S_0) of NO. Assuming that S_0 of NO on hex-Pt(100)[27] at 300 K, where $S_0 = 0.78$, is the same as that for NO on hex-Pt(100) at 100 K, alloyed Sn decreases the S_0 of NO from 0.78 on hex-Pt(100) at 100 K to 0.16 and 0.12 on the c(2 × 2) and $3\sqrt{2}$ alloys, respectively.

Figure 9 directly compares NO-TPD curves for low θ_{NO} (10% of θ_{NO}^{sat}) and saturation coverage (θ_{NO}^{sat}) on each surface at 100 K. This figure illustrates more clearly the other important effect of Sn, that is, reducing the NO desorption temperature due to weaker chemisorption bonding on the surface. Assuming first-order desorption kinetics and using Redhead analysis,[36] we estimate the NO desorption activation energy at low θ_{NO} to be 118 kJ/mol on Pt(100), 55 kJ/mol on the c(2 × 2) alloy, and 48 kJ/mol on the $3\sqrt{2}$ alloy. The 60−70 kJ/mol decrease in desorption energy corresponds to 50% weaker adsorbate−surface bonding. Reductions in the monolayer saturation coverage and desorption activation energy (30−40 kJ/mol) for NO chemisorption on the Sn/Pt(111) alloys compared to Pt(111) were also found in our previous studies.[20]

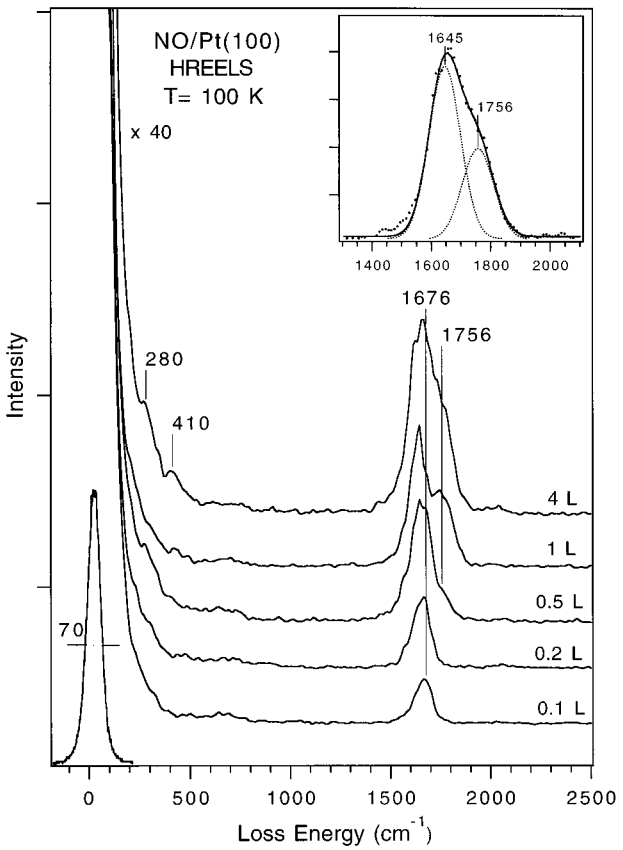

Figure 10. Vibrational spectra from HREELS of NO exposed on hex-Pt(100) at 100 K.

We also investigated NO adsorption on a c(2 × 2)-Sn overlayer ($\theta_{Sn} = 0.5$), prepared by depositing a thin layer of Sn on the hex-Pt(100) surface at 300 K and then annealing to 500 K. The results are shown in Figure 9. NO adsorption was completely eliminated on the Sn adlayer-covered surface at 100 K, even though the surface Sn coverage and Sn−Sn distance were identical to that for the c(2 × 2)-Sn alloy. This clearly illustrates that the site-blocking ability of Sn depends on whether it is present as an adatom or alloyed atom.

3.2. HREELS. Vibrational spectra taken using HREELS are shown in Figure 10 for increasing exposures of NO on hex-Pt-(100) at 100 K. NO was molecularly adsorbed on the hex surface at 100 K without decomposition at all coverages. At low coverage, a single ν_{NO} peak occurred at 1676 cm^{-1}, which shifted to 1645 cm^{-1} with increasing exposures. At higher coverages, an additional band appeared at higher energy. The inset shows a decomposition of the broad ν_{NO} peak obtained for saturation exposures of NO on Pt(100), into two peaks at 1645 and 1756 cm^{-1}. These spectra are consistent with those reported previously.[15,29] The shift of ν_{NO} to lower energy with increasing NO exposures is contrary to the behavior expected on the basis of dipole−dipole interactions.[37] IRAS experiments, by Gardner et al.,[29] showed that the 1676 cm^{-1} band exhibited a positive dipole shift, but it was later replaced at higher NO

TABLE 1: Vibrational Energies (cm^{-1}) of Adsorbed NO for a Saturation Dose of NO on Pt(100) and Sn/Pt(100) at 100 K

	NO/Pt(100)[15]		NO/Pt(100) (this work)		NO/Sn/Pt(100) alloys (this work)		
mode assignment	bent atop	linear atop	bent atop	linear atop	bridged	bent atop	linear atop
ν (Pt−NO)	265		280			361	
δ (Pt−NO)	435		410				
δ (NO)					863	612−632	
ν (NO)	1660	1790	1645	1757	1365	1636−1666	1818−1821

coverages by a new band at a lower frequency. Several components appear at different stages during the hex→(1 × 1) phase change.

The assignment of NO adsorption sites using the ν_{NO} energy is problematic. A wide variety of bonding modes for NO are possible because of the presence of the unpaired antibonding electron in the $2\pi^*$ orbital of NO, and the ν_{NO} energies for these various species overlap strongly. A peak at 1645 cm^{-1} has been assigned to NO adsorption at atop sites in a bent configuration because it falls between the energies for linear-atop 1650−2000 cm^{-1} and bridge-bonded 1480−1545 cm^{-1} sites.[38] The band at 1756 cm^{-1} was assigned to NO bound at linear-atop sites,[29] but it is not associated with (1 × 1)-terraces because this band was not observed on the unreconstructed (1 × 1)-Pt(100) surfaces.[29] Apparently, it is also not associated with the hex-phase because the intensity of this band increases with increasing exposures while the area of the hex phase decreases.[29] It has been suggested that this band is due to NO adsorption at kink sites or other defect sites formed at domain boundaries during reconstruction.[29] The two low energy peaks at 280 and 410 cm^{-1} have been assigned as Pt−NO stretching and Pt−NO bending modes, respectively, on the hex-Pt(100) surface.[15,20] All of these mode assignments are shown in Table 1.

Figure 11 shows the effect of annealing on HREELS spectra following a saturation exposure of NO on hex-Pt(100) at 100 K. Heating the sample to 200 K caused a decrease in the intensity of the ν_{NO} peak at 1777 cm^{-1}, and this peak was eliminated by heating the sample to 450 K. The 1656 cm^{-1} peak also shifted to 1586 cm^{-1} upon heating the sample to 450 K. All of the ν_{NO} loss peaks disappeared after the surfaces were heated to 500 K. The value for ν_{NO} of 1586 cm^{-1} is lower than the value observed following a small NO exposure to give a similar NO coverage on a hex-Pt(100) surface at 100 K. This indicates that the hex-Pt(100) surface has been reconstructed to a (1 × 1) structure upon being heated to 450 K in the presence of adsorbed NO. A new peak at 540 cm^{-1} appeared after the surface was heated to 400 K. This peak broadened and was shifted to 590 cm^{-1} and reduced in intensity after the surface was heated to 800 K. We assign this peak to ν_{Pt-O} of oxygen adatoms formed by decomposition of NO, which occurs for $T \geq 400$ K. The broad nature of the peak suggests the presence of two kinds of oxygen atoms on the surface. These data are consistent with the TPD results showing that NO and N_2 have desorbed from the surface by 600 K and oxygen adatoms are almost fully removed from the surface as O_2 by heating it to 800 K.

The HREELS spectra, obtained after increasing NO exposures on the c(2 × 2) alloy at 100 K, are shown in Figure 12. An exposure of 1 langmuir NO produced a peak at 1636 cm^{-1} and two peaks in the lower energy range, at 371 and 632 cm^{-1}. We assign the peak at 632 cm^{-1} to a NO bending mode that is dipole active when NO is adsorbed in a bent (nonlinear or tilted) configuration and the peak at 1636 cm^{-1} to ν_{NO} for NO adsorbed at atop sites in a bent geometry. The 371 cm^{-1} peak can be assigned to a Pt−NO stretching mode ν_{Pt-NO}. A 3 langmuir NO exposure increased the NO coverage and this broadened the ν_{NO} peak and caused a shift of the ν_{NO} peak to 1806 cm^{-1} and the NO bending mode to 672 cm^{-1}. A new peak appeared at 1023 cm^{-1}, but we have no assignment for this peak. A similar peak was found for NO adsorbed on Cu(111)[39] and assigned to a combination mode of (in this case) the 371 and 672 cm^{-1} vibrations. However, a highly inclined NO species, such as that found on Rh(100),[40] could also give a vibrational loss peak at this energy. At saturation NO coverage (6 langmuirs), the Pt−NO stretching band at 361 cm^{-1} became very intense, and the higher energy ν_{NO} peak grew and became the dominant contribution in the broad peak at 1806 cm^{-1} The inset shows a decomposition of this 1806 cm^{-1} peak into two peaks at 1818 and 1694 cm^{-1}. The electron energy loss data alone do not distinguish among the potential origins of the two ν_{NO} peaks: (i) two different monomeric species, (ii) ν_sNO and ν_{as}NO of a dimer or a dinitrosyl, or (iii) a combination of all of these. Some insight comes from observation of peaks at 1365 and 863 cm^{-1}. The peak at 1365 cm^{-1} falls in the range 1350−1545 cm^{-1} that is typical for NO adsorbed in 2-fold bridge sites. Though pure-Pt 2-fold short bridge sites do not exist on this c(2 × 2) alloyed surface, mixed Pt−Sn 2-fold short bridge sites do exist. This peak might also arise from NO in a bent configuration on the pure-Pt 2-fold long bridge sites. The peak at 863 cm^{-1} was assigned to a bending vibration of bent, bridge-bonded NO. NO bonded to 2-fold bridge sites in a bent configuration has been reported on Cu(111).[39] We attribute the small peak at 2228 cm^{-1} to the N−N stretching vibration of

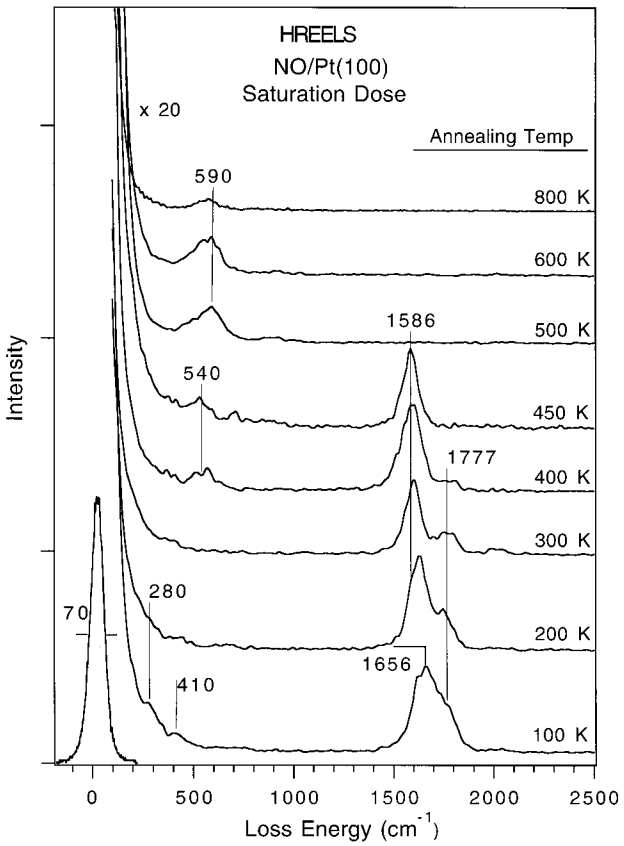

Figure 11. HREELS spectra of NO after sequentially heating to higher temperature following a saturation dose of NO on hex-Pt(100) at 100 K.

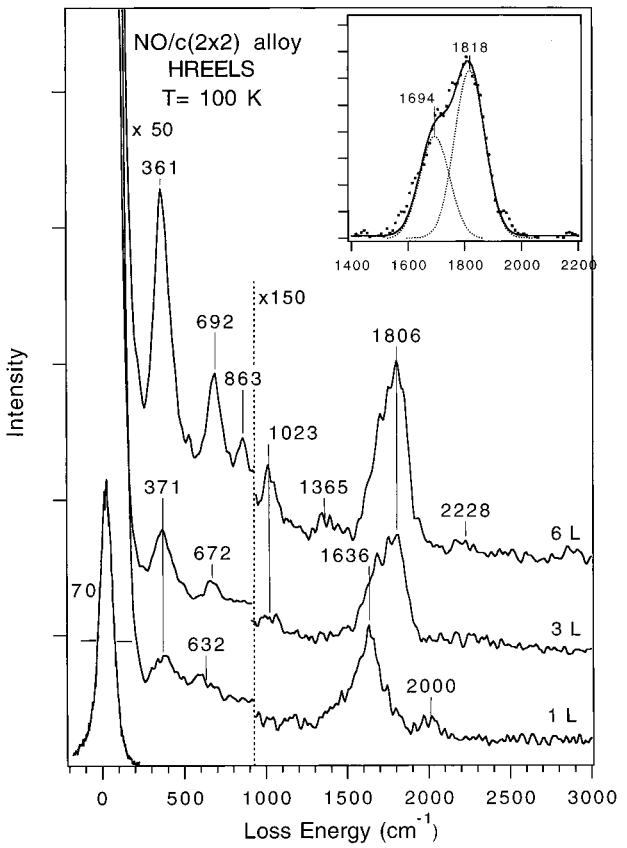

Figure 12. HREELS spectra following NO exposures on the c(2 × 2)Sn/Pt(100) alloy at 100 K.

TABLE 2: Vibrational Energies (cm^{-1}) of N_2O for a Saturation Dose of NO on Sn/Pt(100) Alloy Surfaces at 100 K

mode assignment	$N_2O_{(a)}$/Pt(111)[42]	Sn/Pt(100) alloy (this work)
ν (Pt−N_2O)	325	351−361
δ (NN−O)	575	580
ν (NN−O)	1300	1234
ν (N−NO)	2310	2198−2228

adsorbed N_2O. The N−N−O stretching vibration of N_2O would be expected to cause a peak at 1250 cm^{-1}, but this was not observed here. All of the mode assignments for N_2O are shown in Table 2.

Figure 13 shows HREELS spectra after a monolayer of NO on the c(2 × 2) alloy was sequentially heated to 1000 K. The spectrum taken after the sample was heated to 200 K indicates that molecular NO was still present, adsorbed on the surface. The elastic peak intensity decreased sharply at 200 K, indicating a disordered adlayer and possibly NO dissociation or reaction. Heating the surface to 300 K eliminated the Pt−NO stretching vibration and caused broad loss features, near 460 and 570 cm^{-1}, to appear. This aids the interpretation of the TPD spectra by showing that all of the molecularly adsorbed NO and N_2O species are desorbed or decomposed at this temperature. Further heating the surface to 500 K nearly eliminates the peak at 460 cm^{-1}. The loss peak at 570 cm^{-1} is from Pt−O stretching vibrations because only oxygen adatoms remain at the surface. The elastic peak count rate from this surface was quite high, consistent with a large chemical ordering change. Heating the surface to 1000 K desorbed all of the oxygen as O_2, but it also destroyed the c(2 × 2) alloy structure.

A set of HREELS spectra after NO exposures on the 3√2 alloy at 100 K is shown in Figure 14. At low NO exposures, a

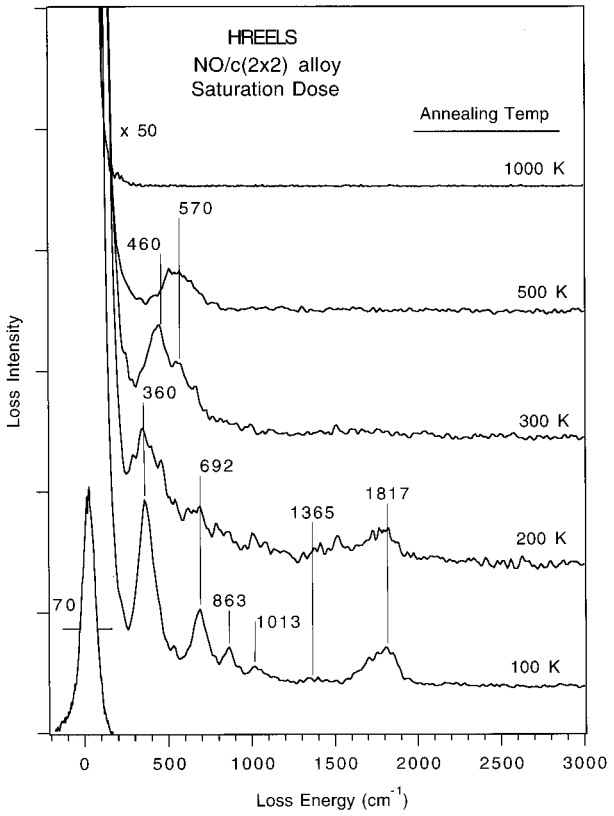

Figure 13. HREELS spectra obtained after stepwise annealing a saturation dose of NO on the c(2 × 2) alloy at 100 K.

ν_{NO} peak was observed at 1666 cm^{-1}. This is higher than that on the c(2 × 2) alloy and close to that on Pt(100). Similar behavior is found for adsorbed CO on these two alloyed surfaces.[41] With increasing NO exposures, the 602 cm^{-1} peak grew larger, and the peak near 1736 cm^{-1} broadened. At saturation coverage, the spectra was dominated by peaks at 351 and 1816 cm^{-1}, with smaller loss peaks at 580, 863, 1234, and 2198 cm^{-1}. Similar to the c(2 × 2) alloy, the inset shows the decomposition of the broad peak at 1816 cm^{-1} to two peaks at 1821 and 1698 cm^{-1}.

On the 3√2 alloy, formation of N_2O from the reaction of adsorbed NO occurs at 100 K. The peaks at 580, 1234, and 2238 cm^{-1} are assigned to the three normal modes of linear N_2O molecules: N−N−O bending (δ_{NNO}), N−N−O stretching (ν_{NNO}), and N−N stretching (ν_{NN}) modes, respectively.[42] These mode assignments are shown in Table 2. This is consistent with the TPD showing the evolution of N_2O and furthermore shows that this reaction occurs at temperature as low as 100 K.

4. Discussion

Alloying the Pt(100) surface with Sn to form the c(2 × 2) and the 3√2 Pt−Sn alloys strongly effects the adsorption and reaction of NO on these surfaces. On hex-Pt(100) at 100 and 300 K, NO is molecularly adsorbed and NO decomposition only occurs at temperatures higher than 400 K.[15−18] On the (1 × 1)-Pt(100) surface at 300 K, NO is partly dissociatively adsorbed on the surface and heating in TPD leads to desorption of N_2, O_2, and NO as the main reaction products.[15−18] Hence, surface structure plays an important role in NO reactions on Pt surfaces. Alloying the Pt(100) surface with Sn to form the c(2 × 2) and 3√2 alloys produces a square-lattice structure similar to that of (1 × 1)-Pt(100), and these surfaces are also more reactive than hex-Pt(100). However, alloying changed the selectivity for

the products formed by thermal reactions of NO on the surface: N_2O, rather than N_2, along with NO and O_2 are the major desorbed species. The reactivity was also enhanced on the c(2 × 2) and $3\sqrt{2}$ alloys: NO adsorption was only 30−40% reversible on the alloys, compared to 75% on the hex-Pt(100) surface. In a related system, on Pt−Rh alloys used as model catalysts for NO reduction, both N_2 and N_2O were formed as reaction products.[43] In those studies, the selectivity toward N_2 and N_2O depended on the relative concentration of NO_{ads} and N_{ads} on the surface and the reaction temperature.

The presence of surface-bound N_2O formed from reaction of NO can account for the peaks at 2228 and 2238 cm^{-1} on the c(2 × 2) and $3\sqrt{2}$ alloys, respectively, in the HREELS spectra of a saturated NO layer along with two other peaks at 580 and 1234 cm^{-1} on $3\sqrt{2}$ alloy. This conclusion is based on spectra following N_2O adsorption on Pt(111)[42] and N_2O formation from NO reactions on Ag(111)[44,45] and Mo(110).[46] All of the mode assignments for our spectra are shown in Table 2. TPD data showed that N_2O was produced and desorbed from these two Pt−Sn alloys, and HREELS shows furthermore that N_2O is formed at 100 K.

We consider below two possible mechanisms for N_2O formation on the two Sn/Pt(100) alloys. The first is a dissociative mechanism:

$$NO_{(a)} \rightarrow N_{(a)} + O_{(a)} \quad (1)$$

$$N_{(a)} + NO_{(a)} \rightarrow N_2O_{(a)} \quad (2)$$

$$2N_{(a)} \rightarrow N_{2(g)} \quad (3)$$

$$2O_{(a)} \rightarrow O_{2(g)} \quad (4)$$

The second mechanism involves dimerization:

$$2NO_{(a)} \rightarrow (NO)_{2(a)} \quad (5)$$

$$(NO)_{2(a)} \rightarrow N_2O_{(a)} + O_{(a)} \quad (6)$$

$$2O_{(a)} \rightarrow O_{2(g)} \quad (7)$$

In the dissociative mechanism, $N_{2(g)}$ may also desorbed depending on the relative rates of the reactions 2 and 3.

Alloying Sn into the Pt(100) surface causes a large reduction in the heat of adsorption of NO, that is, the Pt−NO bond strength. The desorption activation energy, which is equal to the adsorption energy for nonactivated adsorption, decreases from 118 kJ/mol on hex-Pt(100) to 55 kJ/mol on the c(2 × 2) alloy and 48 kJ/mol on the $3\sqrt{2}$ alloy. Hence, it is unlikely that these alloys would be more reactive for dissociation of NO at lower temperatures. TPD also showed no N_2 desorption from these two alloys, which might occur for a dissociative mechanism. Thus, we favor the dimerization reaction mechanism for N_2O formation on these two Pt−Sn alloys.

Several possible configurations of adsorbed NO at different sites are shown in Figure 15a. At low coverages, NO is adsorbed with a tilted or bent geometry at atop sites on hex-Pt(100) at 100 K.[15,18] At high coverages on the Pt(100) surface, some NO is bonded at atop sites in a linear geometry. We found a similar adsorption geometry of NO at lower coverages on both of the Pt−Sn alloys. However, there was a large difference between the vibrational spectra from the two Pt−Sn alloys at saturation coverage. Two peaks appear in the ν_{NO} region at ∼1695 and ∼1820 cm^{-1} on the two alloys. These two modes can be assigned as atop NO in bent and linear configurations, respectively, as was done previously on Pt(100) surfaces at high coverages.[15,17,18] But, the frequencies and intensity ratios of these

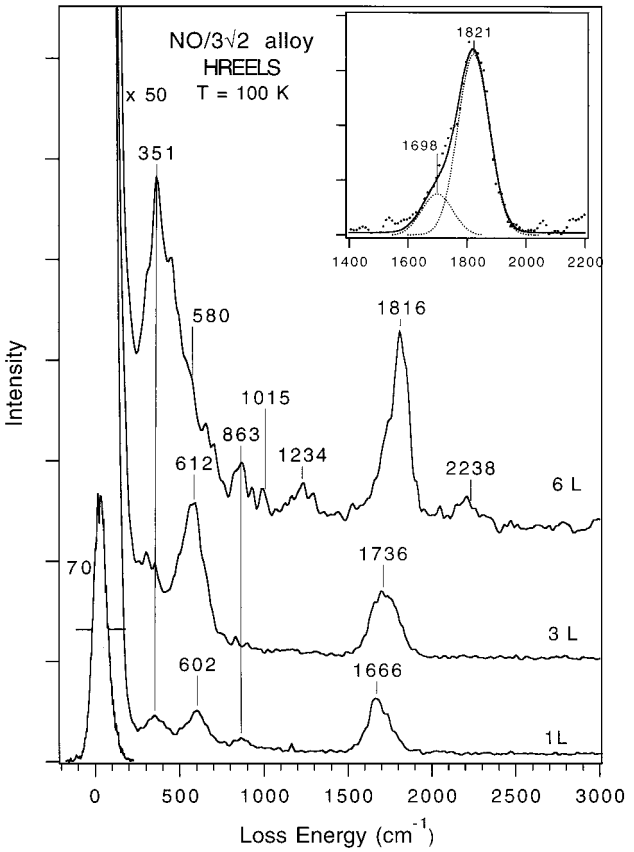

Figure 14. HREELS spectra after NO exposures on the ($3\sqrt{2} \times \sqrt{2}$) R45°Sn/Pt(100) alloy at 100 K.

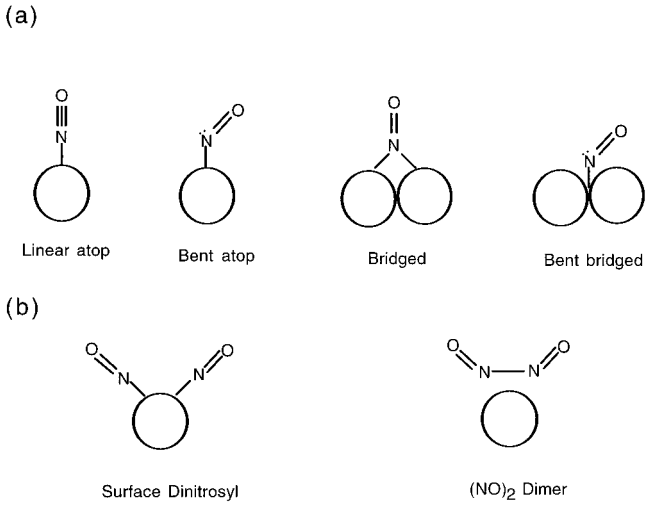

Figure 15. Schematic representation of models for (a) monomeric NO species adsorbed at different sites and (b) dimeric NO species adsorbed as surface dinitrosyl and $(NO)_2$ dimer configuration.

two peaks are quite different on the alloyed surfaces than on Pt(100), and it is therefore worthwhile to consider other possibilities.

On both Ag(111) and Cu(111) surfaces at 90 K, a surface-bound NO dimer $(NO)_2$ is formed.[45,47] The characteristic frequencies for the NO symmetric (ν_sNO) and asymmetric (ν_{as}-NO) stretching modes are 1863 and 1788 cm^{-1}.[43] Dimeric NO species have also been observed with IR on supported catalysts containing tungsten, chromium, and molybdenum with typical values of ν_sNO at 1820 cm^{-1} and ν_{as}NO at 1710 cm^{-1}.[48] These latter dimeric species have been identified as dinitrosyls, in which two NO monomers are bound to a single metal atom

TABLE 3: Vibrational Energies (cm^{-1}) of the Dinitrosyl Intermediate on Sn/Pt(100) Alloys after a Saturation Exposure of NO at 100 K

mode assignment	$(NO)_2$ dimer (I) Ag/(111)[44]	dinitrosyl complex (II) Mo(110)[46]	Sn/Pt(100) (this work)
ν_a (NO)	1788	1720	1694−1698
ν_s (NO)	1863	1821	1818−1821

without the N−N bonding that would be present in an actual dimer, by analogy to polymeric dichlorodinitrosyl-molybdenum and tungsten complexes, which have similar ν_sNO and ν_{as}NO frequencies.[48] Schematic representation of adsorbed dinitrosyl and dimeric species are presented in Figure 15b. If $(NO)_2$ species have C_{2v} symmetry, that is, the two N−O bonds are tilted at equal angles from the surface normal, the ν_{as}NO stretch will be dipole forbidden.[48] However, if the surface dinitrosyl species has C_s symmetry, with the two N−O bonds having different tilt angles, the ν_{as}(NO) mode will be dipole allowed. (This may, however, still give a weak dynamic dipole, relative to ν_sNO, and thus may be difficult to detect.) On Mo(110), from isotopic shifts in IR, a dinitrosyl intermediate with ν_sNO at 1821 cm^{-1} was identified for N_2O formation from NO reaction at low temperatures.[46] Mode assignments for the surface dimer and dintrosyl species are given in Table 3.

In our spectra on the two alloyed surfaces, NO vibrations at ∼1820 cm^{-1} and ∼1695 cm^{-1} are significantly perturbed from that of $(NO)_2$ dimeric species ν_sNO (1863 cm^{-1}) and ν_{as}NO (1788 cm^{-1}) on the weakly interacting Ag(111) and Cu(111) surfaces.[45,47] But 1820 and 1695 cm^{-1} are very similar to the vibrations of a surface dinitrosyl complex with ν_sNO (1820 cm^{-1}) and ν_{as}NO (1710 cm^{-1}). We propose that a surface dinitrosyl complex, in which two NO molecules are bound to one Pt site, is an intermediate for low-temperature N_2O formation on these two Sn/Pt(100) surface alloys. The intensity ratio of these two peaks indicates that the two NO molecules in the dinitrosyl species are tilted with different tilt angles from the surface normal, and thus, the ν_{as}NO mode is dipole allowed. (A tilted monomeric species at atop sites can also contribute to the 1695 cm^{-1} peak.)

On the c(2 × 2) alloy, each Pt atom is surrounded by Sn atom nearest neighbors. Elimination of pure Pt 2-fold and 4-fold hollow sites also suggests the formation of dinitrosyl species (two NO molecules bound to one Pt atom) as intermediates for N_2O formation from adsorbed NO. Hence, N_2 formation from the dissociation of NO requires an ensemble of at least two Pt atoms that do not exist on these alloyed surfaces. Although a detailed IR study, including isotopic shift data, is required for an unequivocal identification of a surface-bound dinitrosyl species, our data suggests that the absence of the adjacent strong bonding sites, which exist for NO on pure Pt surfaces, leads to the formation of a dinitrosyl complex, which subsequently decomposes to form N_2O.

An NO stretching frequency of 1666 cm^{-1}, at low coverage on the $3\sqrt{2}$ alloy, is close to that on the hex-Pt(100) surface and higher energy than on the c(2 × 2) alloy (1636 cm^{-1}). This is surprising because ISS and AES indicate a higher Sn concentration on the $3\sqrt{2}$ alloy.[31,32] Also, the relative amount of molecular NO desorption (40%) is higher on the $3\sqrt{2}$ surface than that (30%) on the c(2 × 2) alloy. This could be due to a weaker Pt−NO bond strength or some special arrangement of Pt and Sn atoms in the $3\sqrt{2}$ alloy. In a similar study of CO adsorption, the ν_{CO} frequency for the $3\sqrt{2}$ alloy was closer to that on Pt(100) than the ν_{CO} on the c(2 × 2) alloy.[41] Both of these results are likely due to a special arrangement of Pt and Sn atoms on the $3\sqrt{2}$ alloy because benzene formation from the cyclotrimerization of acetylene only occurred on the $3\sqrt{2}$ alloy and not on the c(2 × 2) alloy.[49] This reaction is highly structure sensitive and indicates the formation of "(111)-like" sites on the $3\sqrt{2}$ alloy.

It is informative to compare the results for NO adsorption on these two Sn/Pt(100) alloys to those on Sn/Pt(111) alloys.[20] The saturation monolayer coverage of NO on Pt(111) at 100 K is 0.5 ML, and this decreased to 0.4 ML on the (2 × 2)Sn/Pt-(111) alloy and 0.3 ML on the ($\sqrt{3}$ × $\sqrt{3}$)R30° Sn/Pt(111) alloy at 100 K. On Pt(100) at 100 K saturation, the monolayer coverage of NO is 0.73 ML, and this decreased to 0.35 ML on the c(2 × 2)Sn/Pt(100) alloy and 0.22 ML on the ($3\sqrt{2}$ × $\sqrt{2}$)-

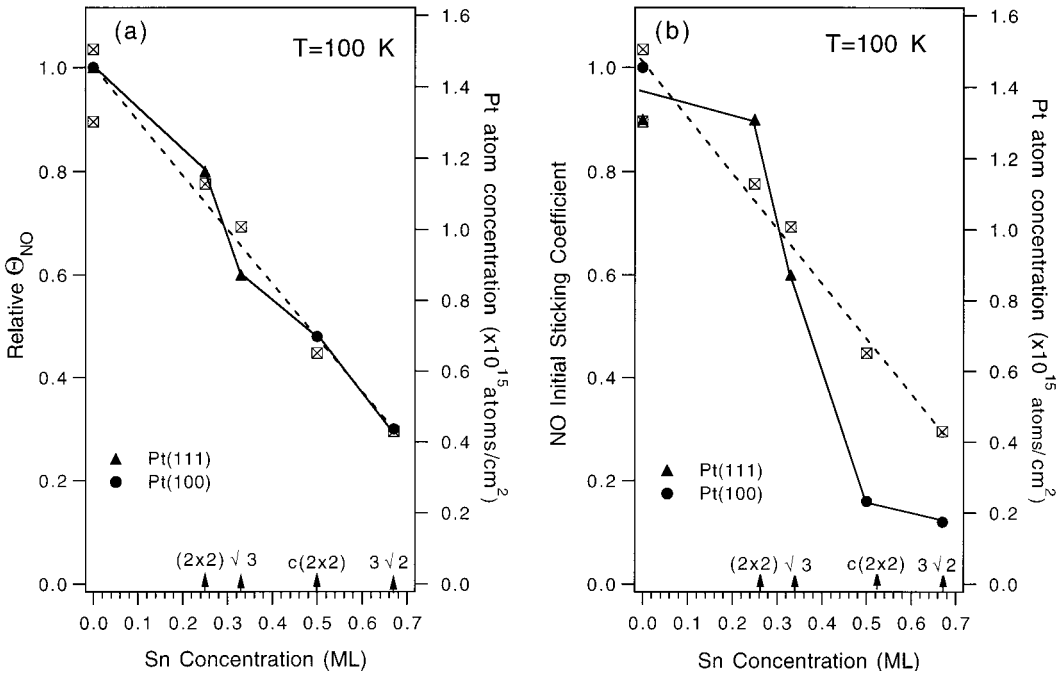

Figure 16. Comparison of (a) normalized NO saturation coverage and (b) initial sticking coefficient S_o of NO on Pt surfaces and several Pt−Sn surface alloys at 100 K. The concentration of Pt atoms in the surface layer is shown with the dashed line and scaled on the right-hand side.

R45° Sn/Pt(100) alloy at 100 K.[20,29] These results are shown in Figure 16 a. We have normalized the monolayer coverage to 1.0 for both Pt(111) and Pt(100). The Pt atom concentration in each surface layer is also plotted on the right-hand side and represented by the dashed line. Figure 16b shows similar curves for S_0(NO) on these surfaces at 100 K. These figures provide a qualitative guide to the influence of alloyed Sn on NO chemisorption over a wide range of Sn concentrations. The NO monolayer coverages and initial sticking coefficients are reduced by alloyed Sn but not necessarily in proportion to the surface Sn concentration. Similar results were obtained for CO[41,50] and C_2H_2[51,49] adsorption on Sn/Pt(100) and Sn/Pt(111) alloys. Under many conditions, a simple Langmuirian site-blocking model for the dependence of the saturation coverage and initial sticking coefficient on modifier coverage fails. Nonlinear behavior in θ_{NO}^{sat} with θ_{Sn} can be understood if the molecular size exceeds the ensemble requirement for adsorption.[52] In such cases, the saturation coverage on the clean (unalloyed) surface is not determined by the adsorption ensemble size but rather by the molecular size. An explanation for the behavior of S_0 has been given that describes the important influence of a "modifier precursor" state on the adsorption kinetics.[53,54] This factor allows for faster adsorption kinetics than expected for a linear decrease in S_0 with increasing modifier coverage.

Adsorption and reaction of NO on these Sn/Pt(111) and Sn/Pt(100) surface alloys are structure sensitive. The activity for decomposition and selectivity of the NO reactions to produce N_2O depends on the surface geometry and the availability of Pt−Pt nearest neighbors on the surface. NO adsorption is completely reversible on Pt(111)[16,19] and Sn/Pt(111) alloys,[20] but substantial NO decomposition occurs on Pt(100)[15−18] and Sn/Pt(100) alloy surfaces (due to the higher heat of adsorption of NO on the (100) plane).

As a final comment that may be helpful in understanding the chemistry of NO, we note that NO is isoelectronic with CO^-, and this additional electron in the antibonding $2\pi^*$ orbital makes NO a weaker π acceptor ligand and a much more versatile ligand than CO. For example, the adsorption energy of CO on the Sn/Pt(100) alloy surfaces is only decreased by 12−16 kJ/mol, compared to Pt(100).[41] In contrast, NO is chemisorbed more weakly, by 60−70 kJ/mol, on these two-alloy surfaces, compared to Pt(100). Also, while the adsorption of CO on Pt(100) and the two Sn/Pt(100) alloys is completely reversible, a substantial change occurs in the NO chemistry on Sn/Pt(100) surfaces due to the presence of Sn. On Pt(100), about 25% of the NO monolayer decomposes to eventually desorb N_2 and O_2. In the presence of Sn, on the two alloys, N_2O formation occurs from NO reaction at very low temperatures, even at 100 K. We believe that this reactivity is due to the low temperature formation of an NO dinitrosyl complex that facilitates N_2O formation.

4. Conclusion

Adsorption and reaction of NO on hex-Pt(100) and two Sn/Pt(100) surface alloys was investigated, primarily by using TPD and HREELS. On hex-Pt(100), NO molecularly adsorbed on the surface at 100 K and then partially (25%) decomposed during heating in TPD to eventually desorb N_2 and O_2. On hex-Pt(100) at 100 K, NO mostly adsorbed at atop sites in a bent configuration with some linearly adsorbed atop NO at higher coverages.

Alloying Sn into the Pt(100) surface to form the c(2 × 2) Sn/Pt(100) and the ($3\sqrt{2} \times \sqrt{2}$)R45° Sn/Pt(100) alloys with $\theta_{Sn} = 0.50$ and 0.67, respectively, has large effects on the adsorption and reaction of NO. Alloying completely changed the selectivity of NO reactions to produce mostly N_2O and O_2 as the reaction products. N_2O formation occurs at very low temperatures, even at 100 K. About 60−70% of the adsorbed NO in the monolayer follows this pathway on these alloyed surfaces. At low coverages on these two alloys, NO adopts the same bent-atop configuration as on hex-Pt(100). However, at higher coverages a surface dinitrosyl complex is formed that we believe to be an intermediate to low-temperature N_2O formation. Alloyed Sn significantly reduced the NO desorption energy, equal in this case to the adsorption energy or Pt−NO bond strength D(Pt−NO), from 118 kJ/mol on hex-Pt(100) to 55 kJ/mol on the c(2 × 2) alloy and 48 kJ/mol on the $3\sqrt{2}$ alloy. The saturation coverage of NO decreased from 0.73 ML on Pt(100) to 0.35 ML on the c(2 × 2) alloy and 0.22 ML on the $3\sqrt{2}$ alloy at 100 K.

Acknowledgment. This work was supported by the US Department of Energy, Office of Basic Energy Sciences, Chemical Sciences Division.

References and Notes

(1) Fisher, T. E.; Kelemen, S. R. *J. Catal.* **1978**, *53*, 24.
(2) Hyden, B. E. *Surf. Sci.* **1983**, *131*, 419.
(3) Kummer, J. T. *J. Phys. Chem.* **1986**, *90*, 4747.
(4) Brown, J. K.; Luntz, A. C. *Chem. Phys. Lett.* **1993**, *204*, 451.
(5) Bünau, G. V.; Wolff, T. *Photochemie*; VCH: Weinheim, 1987; p 178.
(6) Shelef, M. *Catal. Rev.—Sci. Eng.* **1975**, *11*, 1.
(7) Taylor, K. C. *Catal. Rev.—Sci. Eng.* **1993**, *35*, 457.
(8) Hirano, H.; Yamada, T.; Tanaka, K.; Siera J.; Nieuwenhuys, B. E. *Vacuum* **1990**, *41*, 134.
(9) Cobden P.; Nieuwenhuys, B. E. *Surf. Sci.* **1992**, *262*, 97.
(10) Lieske, H.; Volter, J. *J. Catal*. **1984**, *90*, 96.
(11) Srinivisan, R.; De. Angelis R. J.; Davis, B. H. *J. Catal.* **1987**, *106*, 449.
(12) Debauge, Y.; Abon, M.; Bertolini, J. C.; Massardier, J.; Rochefort, A. *Appl. Surf. Sci.* **1995**, *90*, 15.
(13) Hamdaoui, A. E.; Bergeret, G.; Massadier, J.; Primet, M.; Renouprez, A. *J. Catal.* **1994**, *148*, 47.
(14) Banholzer, W. F.; Gohndrone, J. M.; Hatzikos, G. H.; Lang, J. F.; Masel, R. I.; Park, Y. O.; Stolt, K. *J. Vac. Sci. Technol*. **1985**, *A3*, 1559.
(15) Pirug, G.; Bonzel, H. P.; Hopster, H.; Ibach, H. *J. Chem. Phys.* **1979**, *71*, 593.
(16) Gorte, R. J.; Schmidt, L. D.; Gland, J. L. *Surf. Sci.* **1981**, *109*, 367.
(17) Schwartz, S. B.; Fisher, G. B.; Schmidt, L. D. *J. Phys. Chem*. **1988**, *92*, 389.
(18) Zemlyanov, D. Yu; Smirnov, Y.; Gorodetskii, V. V. *React. Kinet. Catal. Lett.* **1994**, *53*, 97.
(19) Ibach, H.; Lehwald, S. *Surf. Sci*. **1978**, *76*, 1.
(20) Xu, C.; Koel, B. E. *Surf. Sci.* **1994**, *310*, 198.
(21) Heilmann, P.; Heinz, K.; Müller, K. *Surf. Sci*. **1979**, *83*, 487.
(22) Behm, R. J.; Hösler, W.; Ritter, E.; Binnig, G. *Phys. Rev. Lett*. **1986**, *56*, 228.
(23) Guo, X.-C.; Hopkinson, A.; Bradley, J. M.; King, D. A. *Surf. Sci*. **1992**, *278*, 263.
(24) Barteau, M. A.; Ko, E. I.; Madix, R. J. *Surf. Sci.* **1981**, *102*, 99.
(25) Thiel, P. A.; Behm, R. J.; Norton, P. R.; Ertl, G. *J. Chem. Phys*. **1983**, *78*, 7437.
(26) Thiel, P. A.; Behm, R. J.; Norton, P. R.; Ertl, G. *J. Chem. Phys*. **1983**, *78*, 7448.
(27) Yeo, Y. Y.; Vattuone, L.; King, D. A. *J. Chem. Phys*. **1996**, *104*, 3810.
(28) Gardner, P.; Tüshaus, M.; Martin, R.; Bradshaw, A. M. *Vacuum* **1990**, *41*, 304.
(29) Gardner, P.; Tüshaus, M.; Martin, R.; Bradshaw, A. M. *Surf. Sci*. **1990**, *240*, 112.
(30) Radnik, J.; Gitmans, F.; Pennemann, B.; Wandelt, K. *Surf. Sci.* **1993**, *287/288*, 330.
(31) Paffett, M. T.; Logan, A. D.; Simonson, R. J.; Koel, B. E. *Surf. Sci*. **1991**, *250*, 123.
(32) Li, Y.; Koel, B. E. *Surf. Sci.* **1995**, *330*, 193.
(33) Windham, R. G.; Bartram, M. E.; Koel, B. E. *J. Phys. Chem*. **1988**, *92*, 2862.

(34) Hoheisel, M.; Kuntze, J.; Speller, S.; Postnikov, A.; Heiland, W.; Spolveri, I.; Bardi, U. To be published.
(35) Saliba, N. A.; Beck, D. E.; Baur, C.; Koel, B. E. Manuscript in preparation.
(36) Redhead, P. A. *Vacuum* **1962**, *12*, 203.
(37) Crossley, A.; King, D. A. *Surf. Sci*. **1977**, *68*, 528.
(38) Cotton, F. A.; Wilkinson, G. *Advanced Inorganic Chemistry*, 3rd ed.; Wiley & Sons: New York, 1972; p 713.
(39) So, S. K.; Franchy, R.; Ho, W. *J. Chem. Phys*. **1991**, *95*, 1385.
(40) Villarrubia, J. S.; Ho, W. *J. Chem. Phys*. **1987**, *87*, 750.
(41) Panja, C.; Koel, B. E. *Isr. J. Chem*. **1998**, *38*, 365.
(42) Avery, N. R. *Surf. Sci*. **1983**, *131*, 501.
(43) Hirano, H.; Yamada, T.; Tanaka, K. I.; Siera, J.; Cobden, P.; Nieuwenhuys, B. E. *Surf. Sci*. **1992**, *262*, 98.
(44) So, S. K.; Franchy, R.; Ho, W. *J. Chem. Phys*. **1989**, *91*, 5701.
(45) Brown, W. A.; Gardner, P.; King, D. A. *J. Phys. Chem*. 1**995**, *99*, 7065.
(46) Queeney, K. T.; Friend, C. M. *J. Chem. Phys*. **1997**, *107*, 6432.
(47) Anderson, A.; Lassier-Govers, B. *Chem. Phys. Lett*. **1977**, *50*, 124.
(48) Millman, W. S.; Hall, W. K. *J. Phys. Chem*. **1979**, *83*, 427.
(49) Panja, C.; Koel, B. E. Manuscript in preparation.
(50) Paffett, M. T.; Gebhard, S. C.; Windham, R. G.; Koel, B. E. *J. Phys. Chem*. **1990**, *94*, 6831.
(51) Xu, C.; Peck, J. W.; Koel, B. E. *J. Am. Chem. Soc*. **1993**, *115*, 751.
(52) Koel, B. E., to be published.
(53) Johnson, S.; Madix, R. D. *Surf. Sci*. **1979**, *83*, 487.
(54) Jiang, L. Q.; Koel, B. E.; Falconer, J. L. *Surf. Sci*. **1992**, *273*, 273.